Academy of Scientific Research and Technology
27th National Radio Science Conference
Faculty of Electronic Engineering, Menoufia Univ., Menouf, Egypt
16-18 March 2010

Signal Processing Methodologies for Digital Beamforming and Image Reconstruction in Ultrasound Imaging

Mawia A. Hassan [1,2], Ahmed S. Mohamed [1], Abo-Bakr M. Youssef [1], Yasser M. Kadah [1]

[1] *System & Biomedical Engineering Department, Cairo University, Giza, Egypt*
[2] *Biomedical Engineering Department, Sudan University of Science & Technology, Khartoum, Sudan*
E-mail: mah@k-space.org

ABSTRACT

PC-based implementations for sophisticated medical imaging technologies have emerged where powerful multi-core computational ability replaces expensive embedded systems. As expand of our previous work-PC Based Modulator Digital Ultrasound Imaging system-we presented here the processing steps done on the PC side. Two type of array element was described: virtual and physical array elements to form N-channel beamformer. The results shown that virtual array elements was given good results in linear array image reconstruction than physical array elements, because it provides additional number of lines. However, physical array elements shown a good results in linear phase array reconstruction (steering) than virtual array elements, because the active elements number (Aperture) is less than in physical array elements. We applied three windowing functions (Hamming, Blackman, and Kaiser (β=4)) to reduce the side lobes. Moreover, the envelope detection was done and the data was compressed using log compression to a range used for display (8 bits), because the maximum dynamic range of the human eye is in the order of 30 dB. Finally we checked the quality of the image using quantitative entropy measured.

1. Introduction

With the growing availability of high-end integrated analog front-end circuits, distinction between different digital ultrasound imaging systems is determined almost exclusively by their software component. Our previous work concerned on description the digital ultrasound imaging system in figure 1 [1]. In this work we concerned on the processing steps which done on the PC side.

A commonly used approach to image acquisition in ultrasound system is digital beamforming. Digital beamforming, as applied to the medical ultrasound, is defined as phase alignment and summation [2] of signals that are generated from a common source, by received at different times by a multi-elements ultrasound transducer [3].

The commonly use arrays are linear, curved, or phase array. The important distinctions arise from the method of beam steering use with these arrays. For linear and curve linear, the steering is accomplished by selection of a group of elements whose location defines the phase center of the beam. In contrast to linear and curve linear array, phase array transducer required that the beamformer steers the beam with switched set of array elements [4]. These requirements mention important differences in complexity over the linear and curved array. Beamformer has two functions: directivity to the transducer (enhancing its gain) and defines a focal point within the body, from which location of the returning echo is derived.

The beamforming process needs a high delay resolution to avoid the deteriorating effects of the delay quantization lobes on the image dynamic range and signal to noise ratio (SNR) [5]. If oversampling is used to achieve this timing resolution [6], a huge data volume has to be acquired and process in real time. This is usually avoided by sampling just above the Nyquist rate and interpolating to achieve the required delay resolution [5].

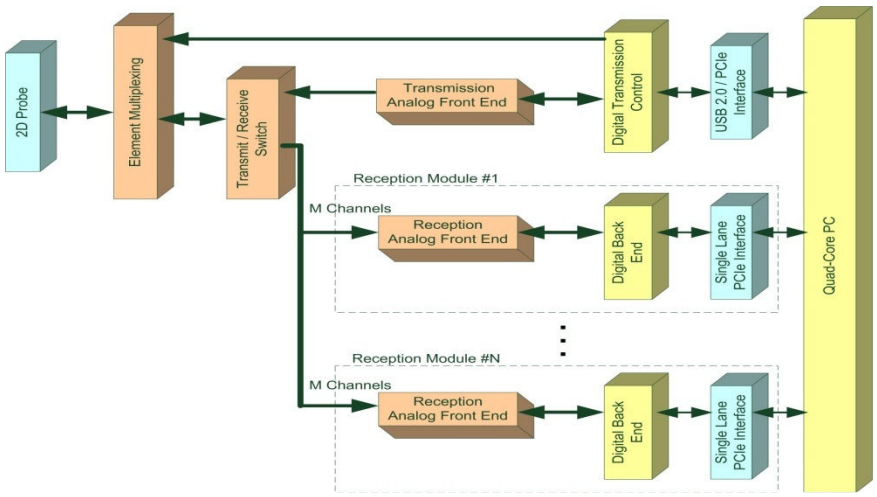

Figure 1. Block diagram of proposed digital ultrasound imaging system

Beamforming required Apodization weighted to decreasing the relative excitation near the edges of the radiating surface of the transducer during transmit or receiving, in order to reduce side lobes.

After delay and sum the envelope of the signals is detected. The envelope then compressed logarithmically to reduce the dynamic range because; the maximum dynamic range of the human eye is in the order of 30 dB [7]. The actual dynamic range of the received signal depends on the ADC bits, the time gain compensation (TGC) amplifier used in the front end, and the depth of penetration. The signal is compressed to fit the dynamic range used for display (usually 7 or 8 bits). It is typical to use a log compressor to achieve the desired dynamic range for display [8].

2. Methodology

1.2 Over sampling technique

Over sampling is used to achieve high delay resolution. However, this increase the data volume has to acquire. This is usually avoided by sampling just above the Nyquist rate and interpolating to achieve the required delay resolution. Radial sampling resolution is derived in:

$$d/N=c/2f_s, \quad (1)$$

where f_s is the sampling frequency in MHz, d is the depth in cm, N is the number of delay values, and c is the speed of sound in m/s. With time resolution T_s:

$$T_s = 1/f_s. \quad (2)$$

From the literature [5], wide band transducer required delay resolution in order of 1/16 the signal period.

2.2 Delay equation

Figure 2 shows the geometry which is used to determine the channel and depth-dependent delay of a focused transducer array. After a wave-front is transmit into the medium an echo wave propagates back from the focal points (P) to the transducer. Which c denoting the speed of sound in the medium, the distance from P to the origin is given by [9]:

$$t_i = \frac{1}{c}\sqrt{(x_i - x_f)^2 + (y_i - y_f)^2}\,, \tag{3}$$

where (x_f, y_f) is the position of the focal point, (x_i, y_i) is the center for the physical element number i, and c is the speed of sound. A point is selected on the whole aperture (AP) as a reference (x_c, y_c) for the imaging process. The propagation time (t_c) for this was calculated as in equation (3), but the distance here from P to the reference (x_c, y_c). The delay to use on each element of the array is then [9]:

$$\Delta t_i = t_c - t_i\,. \tag{4}$$

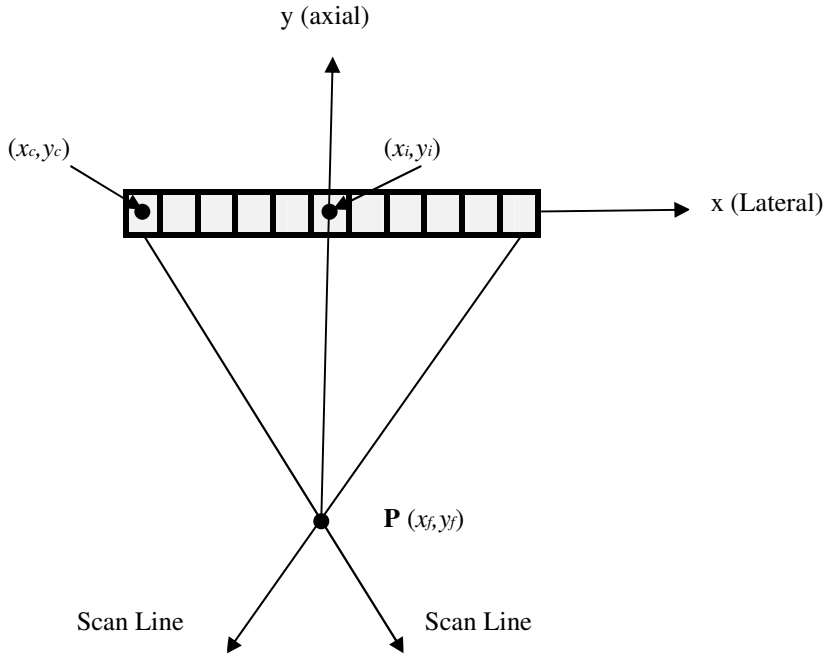

Figure 2. Geometry of a focused transducer array

2.3 physical Array Elements

2.3.1 Linear Array Reconstruction. Selected of a group of elements (aperture) whose location is defines the phase center of the beam [10]. Electronic focusing was applied on receive for each aperture. Received at the aperture elements are delayed by focusing delays and summed to form scan line in the image. After that one elements shift is applied to the aperture and the process was repeated till the end of the array elements at the outer side processing all image scan lines (Figure 3 where aperture equal 32 elements). Number of lines is given by:

Number of lines=Total number of elements - Number of the aperture elements + 1. (5)

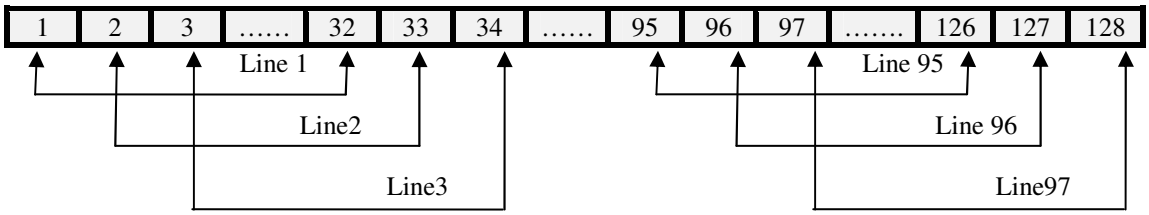

Figure 3. Linear physical array elements

2.3.2 Linear phase array reconstruction. In contrast the linear array, phase array transducer required that the beamformer steered the beam with an unswitched set of array elements [10]. In this process, the time shifts follow a linear pattern across of array from one side to another side. In receive mode, the shifted signals are summed together after phase shift and some signal conditioning to produce a single output. This reconstruction technique divides the field of view (FOV) into different point targets (raster points), P(i,j). Each point represented as an image pixel, which is separated laterally and axially by small distances. Each target is considered as a point source that transmits signals to the aperture elements as in figure 4. The beamforming timing is then calculated for each point based on the distance R between the point and the receiving element, and the velocity of ultrasonic beam in the media. Then the samples corresponding to the focal point are synchronized and added to complete the beamforming as the following.

$$P_D(i,j) = \sum_{n=1}^{N} X_n\left(K_{i,j}\right) \quad , \tag{6}$$

where P_D (i,j) is the signal value at the point whose its coordinates are (i,j), and X_n ($K_{i,j}$) is the sample corresponding to the target point in the signal X_n received by the element number n. The sample number $K_{i,j}$ which is equivalent to the time delay is calculated using the equation below:

$$K_{i,j} = \frac{R_n(i,j)}{T \times c} . \tag{7}$$

Here R_n (i, j) is the distance from the center of the element to the point target, c is the acoustic velocity via the media, and T is the sampling period of the signal data.

2.4 Virtual Array Elements

2.4.1 Linear Array Reconstruction. In this technique we used central elements and assumed there were virtual elements on the left of the central element. For example, if we want to used aperture equal 128 elements we take element number 1 as center element and selected 64 physical elements on the right (already exist) and 64 virtual elements on the left (not exist), as in Figure 5.
To compensate the loss in energy, we multiplied by factor (Ma) because this line really taken from 64 elements instead of 128 elements. The Ma factor equal the number of aperture elements divided by the number of the physical elements.

Image line was obtained from the summation of physical elements multiplied by Ma factor. There for the Line number one equal the summation of the 64 physical elements × 128/64. Then one elements shift was applied to the virtual and physical aperture and this process is repeat till the factor equal 128/128.

2.4.2 Linear phase array reconstruction. We used the same techniques as in section (2.3.2).

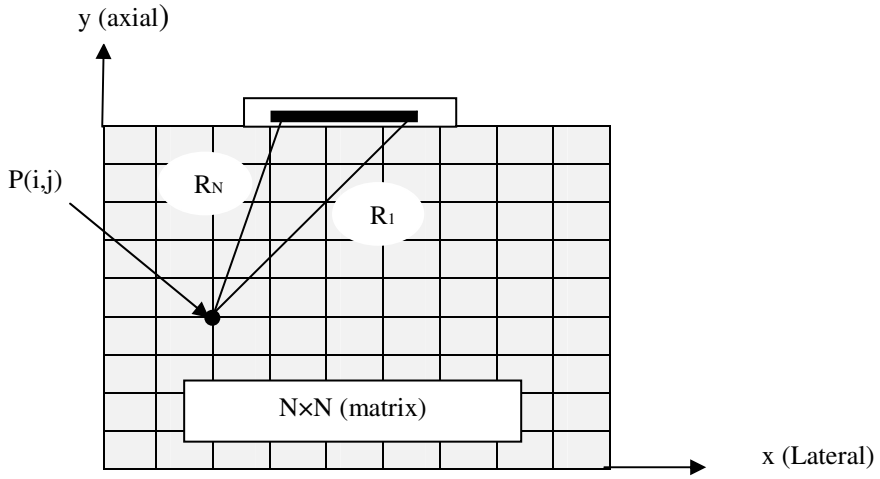

Figure 4. The raster point technique

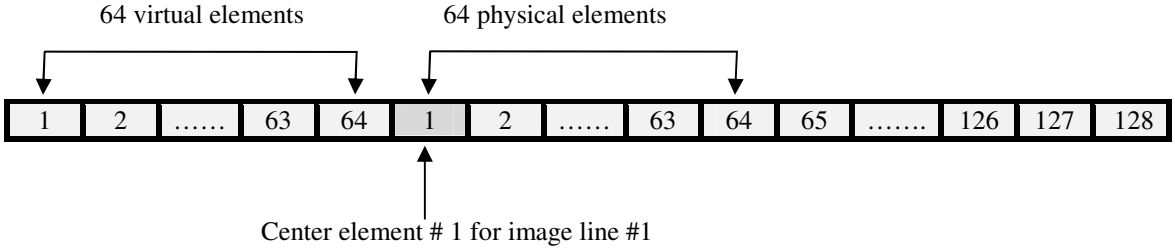

Figure 5. Linear virtual array elements

2.5 Apodization

Apodization is amplitude weighting of normal velocity across the aperture [7], one of the main reasons for apodization is to lower the side lobes on either side of the main beam [11]. Just as a time side lobes in a pulse can appear to be false echoes [7]. Aperture function needed to have rounded edges that taper toward zero at the ends of the aperture to create low side lobes levels. We used windowing functions (hamming, Blackman, and Kaiser (β=4)) as apodization functions to reduce the side lobes. There is trade-off in selecting these functions: the main lobe of the beam broadens as the side lobes lower [7].

2.6 Envelope detection and compressed dynamic range

After delay and sum, the analytic envelope of the signal is calculated as the square root of the sum of the squares of the real and quadrature components [12]. The most accurate way of obtaining the quadrature components was to pass the echo signal through a Hilbert transform [13], because it provides 90-degree phase shift at all frequencies [14].

The envelope then compressed logarithmically to achieve the desired dynamic range for display (8 bits). It is typical to use a log compressor to achieve the desired dynamic range for display. Log transformation compressed the dynamic range with a large variation in pixels values [15].

3. Results and Discussions

3.1 The Ultrasound data

We used correct real data obtained from the Biomedical Ultrasound Laboratory, University of Michigan; the data set that was used to generate the results here is under "Acusonl7". The parameters for this data set are as follows: the number of channels was 128 channels, and the A/D sampling rate was 13.8889 MSPS. Linear shape transducer was used to acquire the data with center frequency of 3.5 MHz, and element spacing of 0.22mm. Each ultrasonic A-scan was saved in a record consisted of 2048 RF samples per line each represented in 2 bytes, and the signal averages was 8. The speed of the ultrasound in the phantom was 1480 m/sec. The data were acquired for phantom within 6 pins at different positions. The data was used to simulate the N-channel beamformer on receive as discussed in methodologies. The radio frequency (RF) signals, A-scan, were recorded from every possible combinations of transmitter and receiver for all elements in the 128 elements.

3.2 Over sampling technique

Table 1 shown the effect of oversampling to the delay resolution. As can be saw when sampling ratio increased the delay resolution decreased according to the radial sampling resolution. From the table it was possible to write:

$$\text{Radial Sampling ratio} = \text{Delay resolution} \times T_s \times c. \quad (8)$$

from the table we take sampling ratio (F) equal 8 as an interpolation factor, and it gave better delay resolution (1/16) the signal period.

Table.1 The effect of the oversampling to the delay resolution

Sampling frequency(F_s)	**Sampling period ($T_s=1/F_s$)**	**Radial sampling resolution($=T_s/2\times c$) Delta-distance(D_d) c=1.480mm/µsec**	**Delay resolution (1/2×sampling ratio)**
F_s=13.8889 Sampling Ratio=1	T_s=72 nsec	D_d=0.0533 mm/samples	1/2
F_s=2×13.8889=27.7778 Sampling Ratio=2	T_s=36 nsec	D_d=0.0267 mm/samples	1/4
F_s=4×13.8889=15.5556 Sampling Ratio=4	T_s=18 nsec	D_d=0.0133 mm/samples	1/8
F_s=8×13.8889=111.1112 Sampling Ratio=8	T_s=9 nsec	D_d=0.0067 mm/samples	1/16

3.3 Physical Elements Array

3.3.1 Linear Array Image Reconstruction. In this situation we reconstructed an image using N-channel beamformer on receive where N=32 and 64. In figure 6 shown two images reconstructed for six pin phantom by linear technique (figure 3). In figure 6 (a and b) the images was reconstructed with focusing using aperture equal 32 and 64 so it is obvious to see more improvement in the lateral resolution where aperture equal 64, because increasing the size of the aperture improve the lateral resolution. However, the (FOV) was reduced in aperture equal 64 more than 32.

3.3.2 Linear Phase Array Reconstruction. Due to the small FOV of the linear reconstruction and its limited lateral resolution, we used linear phase reconstruction to reconstructed image of six pins phantom from the data set. Figure 7 shown images reconstructed using raster point technique. Element number 128 was the transmitter and received with all 128 elements. In figure 7 (a and b) image was reconstructed using F equal 4 and 8. As we shown when F increase improve the image quality because from table 1 radial resolution equal 0.0067 for (F=8) compared to 0.0133 for (F=4). Figure 8 shown image reconstructed by the same technique

using all elements for transmitted and received. The six pin of the phantom are clearly described with a moderate lateral resolution.

(a) (b)

Figure 6. Physical Linear array image reconstruction, (a) Using AP=32, (b) Using AP=64

3.4 Virtual Array elements

3.4.1 Linear Array Image Reconstruction. Table 2 shown a comparison between linear array reconstruction with physical and virtual elements, as can be seen virtual elements provide additional scan lines leaded to improved the FOV and lateral resolution than using physical array elements. Also virtual array elements provided a possibility of using Aperture equal 128 elements gave 65 lines and that could not be acceptable in physical array elements, because we had only one line.

(a) (b)

Figure 7. Physical Linear phase array image reconstruction, element number 128 for transmitted and received with all 128 elements, (a) Using F=4, (b) Using F=8

(a) (b)

Figure 8. Physical Linear phase array image reconstruction, transmitted and received with all 128 elements (a) Using F=4, (b) Using F=8

Table 2. Number of lines in linear array image reconstruction with physical and virtual elements

	Physical elements	virtual elements
AP=32	97 lines	113 lines
AP=64	65 lines	97 lines
AP=128	1 lines	65 lines

Figure 9 shown 32, 64, and 128 elements channel beamformers. Figure 9 (a and b) shown 32 and 64 channel respectively, as can be shown, when increased the aperture the lateral resolution was improved and also FOV been better than physical array elements in figure 6 (a and b). In figure 9 (c) the aperture equal 128 which it's unacceptable in physical array elements.

(a) (b) (c)

Figure 9. virtual Linear array image reconstruction, (a) Using AP=32, (b) Using AP=64, (c) using AP=128

3.4.2 Linear Phase Array Reconstruction. In figure 10 (a, b, and c) shown images reconstructed using raster point technique for virtual elements when aperture equal 32, 64, and 128 elements respectively. As we saw virtual elements array in steering reduced the FOV but the lateral resolution was good compared to the physical array elements which gave a good FOV and lateral resolution.

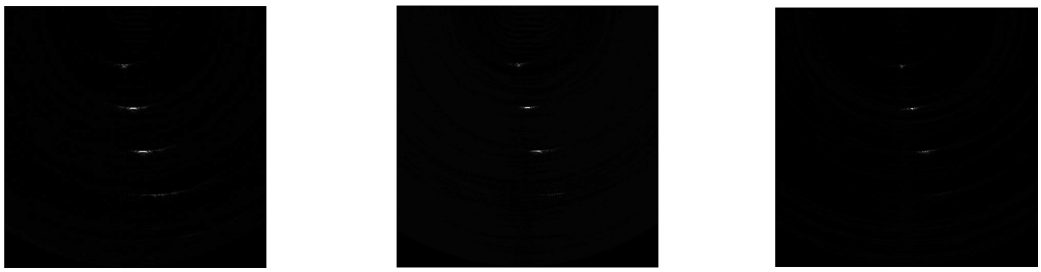

(a) (b) (c)

Figure 10. Virtual Linear phase array image reconstruction, (a) Using AP=32, (b) Using AP=64,(c) AP=128

3.5 Effect of Apodization

Table 3 shown the effect of Hamming, Blackman, and Kaiser (β=4) compared to rectangular window. Because the aperture is rectangular unfortunately, the far field beam pattern is a sinc function with near in-side lobes only -13 dB down from the maximum on axis value.

Table 3. Hamming, Blackman, and Kaiser (β=4) apodization functions compared to rectangular window

Type of Window	Peak Side Lope Amplitude(Relative)	Approximate Width of Main Lobe
Rectangular	-13.3	0.013672
Hamming	-42.6	0.025391
Blackman	-58.1	0.025391
Kaiser (β=4)	-30.0	0.017578

Figure 11 shown a comparison between images reconstructed without apodization using physical array elements (transmitted and received by all elements) to images reconstructed with apodization. As can be shown in figure

11 (b, c, and d) there is trade-off in selecting these functions: the main lobe of the beam broadens as the side lobes lower compared to figure 11 (a) for rectangular aperture.

3.6 Envelope detection and compressed dynamic range

Figure 12 shown comparisons between envelope images used physical and virtual linear array elements. In figure 12(a and b) image reconstructed using aperture equal 32 and 64 with physical array. Moreover, figure 12 (c, d, and e) shown images reconstructed using aperture equal 32, 64, and 128 respectively. As can be shown virtual elements array provide best FOV and lateral resolution than physical array elements and advantaged for using aperture equal 128.

In figure 13 we shown the envelope of images used raster point technique (There were 128 elements for transmits and receives), apodized by Hamming, Blackman, and Kaiser (β=4) respectively. As can be viewed the results were better than figure 11 (b,c, and d), because the envelope provided more signal strength as can be saw in figure 14.The same was also said for figure 12 (a and b) compared to figure 6 (a and b) and figure 12 (c,d, and e) compared to figure 9 (a,b,and c).

(a) (b) (c) (d)

Figure 11. Comparison between images reconstructed with and without apodization. (a) Image without apodization, (b) Image apodized with Hamming,(c) Image apodized with Blackman,(d) image apodized with kaiser (β=4)

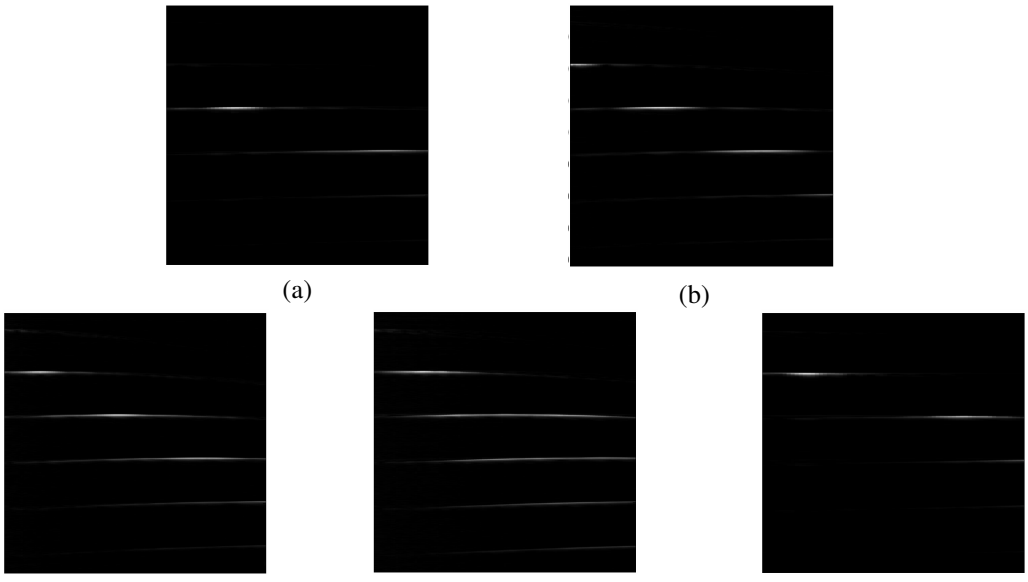

(a) (b)

(c) (d) (e)

Figure 12. comparisons between envelope images used physical and virtual linear array elements (a) Image with physical array elements using AP=32, (b) Image with physical array elements using AP=64, (c) Image with virtual elements using AP=32, (d) Image with virtual elements using AP=64, (e) Image with virtual elements using AP=128,

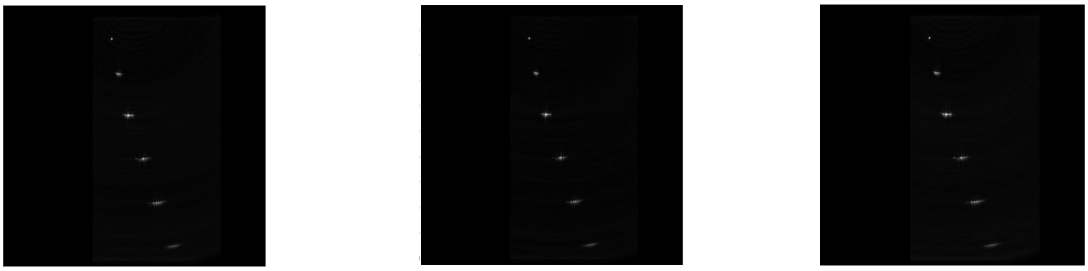

(a) (b) (c)

Figure 13. The envelope images used raster point technique (There were 128 elements for transmits and receives) (a) Envelope image apodized with Hamming , (b) Envelope image apodized with Blackman , (c) Envelope image apodized with Kaiser (β=4)

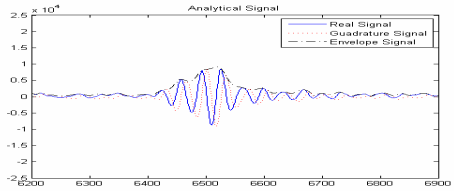

Figure 14. The analytical envelope

Figure 15 (a,b, and c) shown the images in figure 13 (a, b, and c), which compressed the dynamic range using logarithmic compression to achieve the desired dynamic range for display (8 bits).

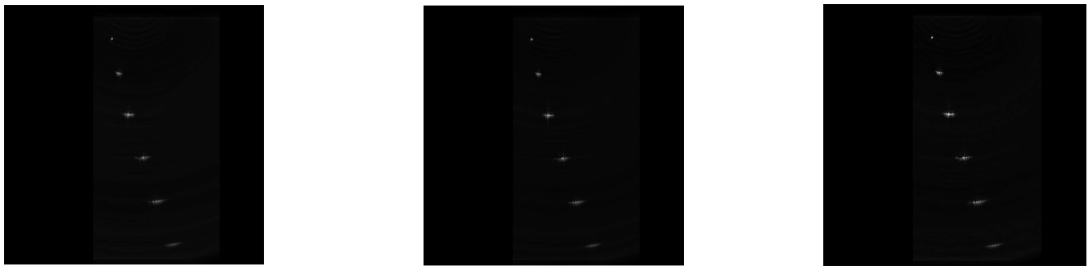

(a) (b) (c)

Figure 15. The compressed envelope images used log compression (transmitted and received with all elements) (a) Compressed envelope image apodized with Hamming , (b) Compressed envelope image apodized with Blackman , (c) Compressed envelope image apodized with Kaiser (β=4)

Figure 16 (a) shown pin three in the compressed image as a sub-image without apodization. Figure 16 (b , c, and d) shown the same pin apodized by Hamming, Blackman, and Kaiser (β=4) respectively. Figure 16 (e, f, and g) was a lateral profiles shown the effect of apodization to the side lobes and main lobe as function in the frequency domain. As can be seen when side lobes suppressed the beam would be prodders.

We selected pin number two and pin number three as sub-images (64X64) and (100X100) respectively, to show the quality of the images using entropy function.

Table 4 shown a comparison of images quality (entropy) without apodization (figure 11 (a)), image with apodization (figure 11 (b)), envelope image with apodization (figure 13 (a), and compressed image with apodization (figure 15(a)). Apodization was done using Hamming window.

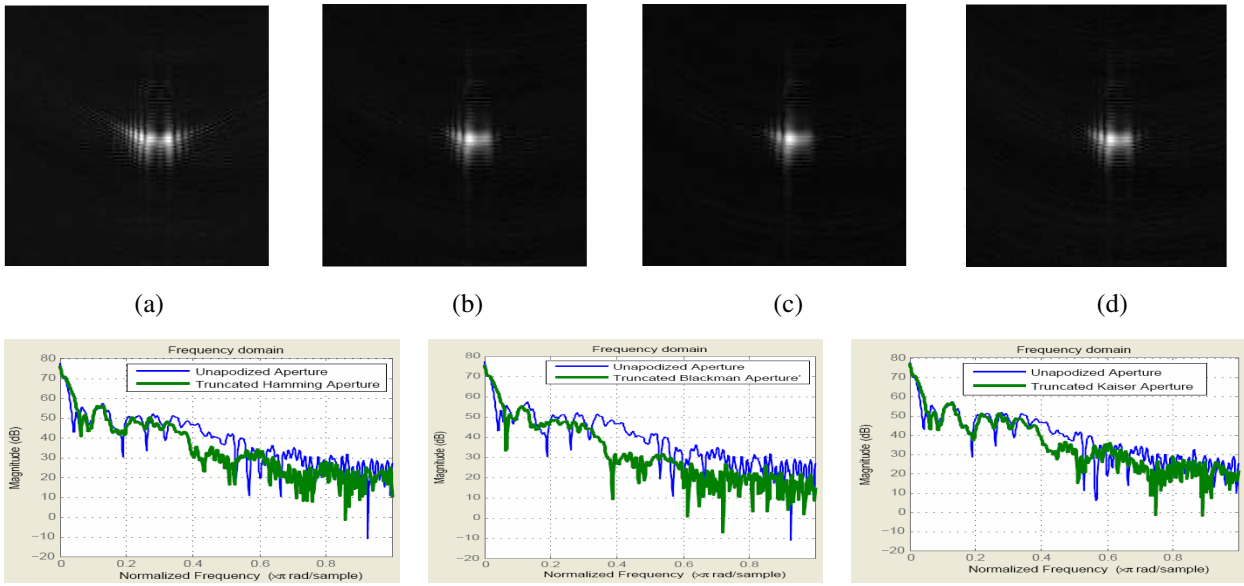

Figure 16. Pin three in the phantom as a sub-image. (a) Without apodization,(b) apodized with Hamming , (c) apodized with with Blackman , (d) apodized with Kaiser (β=4), (e) Fourier spectrum of figure 16 (b), (f) Fourier spectrum of figure 16 (c), (e) Fourier spectrum of figure 16 (d)

Table 4. Entropy of sub-images with apodization (Hamming) and without apodization

	Without Apodization	With Apodization	Compressed with Apodization	Compressed without Apodization
Pin 2	0.3947	0.302	4.1727	4.6636
Pin 3	0.2514	0.2358	3.9452	4.2748

Table 5 shown entropy of images without apodization (figure 11 (a)), image with apodization (figure 11 (c)), envelope image with apodization (figure 13 (b), and compressed image with apodization (figure 15(b))**.** Apodization with Blachman window.

Table 5. Entropy of sub-images with apodization (Blackman) and without apodization

	Without Apodization	With Apodization	Compressed with Apodization	Compressed without Apodization
Pin 2	0.3947	0.2979	3.9682	4.6636
Pin 3	0.2514	0.2455	3.806	4.2748

In Table 6 we shown calculated entropy of images without apodization (figure 11 (a)), image with apodization (figure 11 (d)), envelope image with apodization (figure 13 (c)), and compressed image with apodization (figure 15(c)). Apodization was done using Kaiser (β=4) window.

From the tables entropy of image is minimized when the image was uniform. Image with apodization was given enteropy value less than image without apodization, indicated for suppressed side lopes. Also the compressed image with apodization gave better result than compressed image without apodization. As can be seen Blackman given better results than Hamming and Kaiser in compressed image with apodization.

Table 6. Entropy of sub-images with apodization (Kaiser(β=4)) and without apodization

	Without Apodization	With Apodization	Compressed with Apodization	Compressed without Apodization
Pin 2	0.3947	0.313	4.3319	4.6636
Pin 3	0.2514	0.2377	4.0698	4.2748

4. Conclusion

Signal processing methodologies for digital beamforming and image reconstruction has been presented. Two type of elements array: virtual and physical, has been described. Moreover, the effect of apodization and compressed images used algorithmic compression in each type was mentioned. Finally we checked the image quality using entropy function.

Acknowledgements. We would like to thank Biomedical Ultrasonic's Laboratory, University of Michigan, for making the group's RF data available.

References

[1] A. M. Hendy ,M. A. Hassan, R. Eldeeb, D. Kholy, A. Youssef and Y. M. Kadah, "PC-Based Modular Digital ultrasound Imaging system," *in Proc. IEEE Ultrason. Symp*., Rome, Italy, September 2009. (in press).

[2] R.A. Mucci, "A Comparison of Efficient Beamforming Algorithms," *IEEE Trans. Acoustics, Speech, And Signal Proc., vol.* 32. pp. 548-558, 1984.

[3] R. Reeder, C. Petersen, "The AD9271-A Revolutionary Solution for Portable Ultrasound," *Analog Dialogue* 41-07,Analog Devices, July 2007.

[4] K. E. Thomenius, "Evaluation of Ultrasound Beamformers," *in Proc. IEEE Ultrason. Symp.,* pp.1615-1621, 1996.

[5] C. Fritsch, M. Parrilla, T. Sanchez, O. Martinez, "Beamforming with a reduced sampling rate," *Ultrasonics, vol*. 40, pp. 599–604, 2002.

[6] B. D. Steinberg, "Digital beamforming in ultrasound," *IEEE Transactions on Ultrasonics, Ferroelectrics and Frequency Control, vol.* 39, pp. 716–721, 1992.

[7] Szabo, T. L., *Diagnostic Ultrasound Imaging: Inside Out*, Elsevier Academic Press: Hartford, Connecticut, 2004.

[8] M. Ali, D. Magee and U. Dasgupta, "Signal Processing Overview of Ultrasound Systems for Medical Imaging," SPRAB12, Texas Instruments, Texas, November 2008.

[9] J. A. Jensen, "Ultrasound imaging and its Modeling", Department of Information Technology, Technical University of Denmark, Denmark, 2000.

[10] D. A .Christensen, *Ultrasonic Bioinstrumentation*, Jonh Wiley & Sons, New York, 1988.

[11] J. Synnevag, S. Holm and A. Austeng, "A low Complexity Delta-Dependent Beamformer," *in Proc. IEEE Ultrason. Symp., pp.*1084-1087,. 2008.

[12] J. O. Smith, *Mathematics of the Discrete Fourier Transform (DFT),* Center for Computer Research in Music and Acoustics (CCRMA), Department of Music, Stanford University, Stanford, California, 2002.

[13] A. V. Oppenheim and R. W. Schafer, *Discrete-Time Signal Processing*. NJ: Prentice-Hall, Englewood Cliffs, 1989.

[14] B.G. Tomov and J.A. Jensen, "Compact FPGA-Based Beamformer Using Oversampled 1-bit A/D Converters," *IEEE Transactions on Ultrasonics, Ferroelectrics and Frequency Control, vol.* 52, no. 5, pp. 870-880, May 2005.

[15] R. C. Gonzalez, R. E. Woods, *Digital Image Processing*, Pearson Prentice Hall, Upper Saddle River, New Jersey, 2008.